# Experimental study of the $^{24}$Na$^{m}(d, p)\,^{25}$Na reaction and implications for the influence of the $^{24}$Al$^{m}$ isomer on $rp$-process nucleosynthesis

N. Gerken [●], S. Almaraz-Calderon, B. W. Asher, E. Lopez-Saveedra, L. T. Baby, K. W. Kemper,
A. Morelock, J. F. Perello, A. Volya, and I. Wiedenhöver
*Department of Physics, Florida State University, Tallahassee, Florida 32306, USA*

A radioactive beam of $^{24}$Na with 90% of its content in its $1^{+}$ isomeric state ($E_{ex} = 0.472$ MeV, $t_{1/2} = 20.18$ ms) has been developed and used to perform a measurement of the $^{24}$Na$^{m}(d, p)\,^{25}$Na reaction at the John D. Fox Accelerator Laboratory at Florida State University. This reaction selectively populated $\ell = 0$ transfers, allowing the study of low-spin states in $^{25}$Na. Mirror symmetry arguments were then used to investigate the effects of the isomeric state of $^{24}$Al ($E_{ex} = 0.426$ MeV, $t_{1/2} = 130$ ms) on the astrophysical rate of the $^{24}$Al$^{m}(p, \gamma)\,^{25}$Si reaction. Experimental parameters were extracted to provide, for the first time, an experimental reaction rate for the destruction of $^{24}$Al via proton captures in its isomeric state relevant to $rp$-process nucleosynthesis.

## I. INTRODUCTION

The rapid proton-capture ($rp$) process occurs in hot hydrogen-rich environments at temperature in excess of 0.1 gigakelvin (GK) [1]. X-ray bursts [2–4], novae and supernovae outbursts [1], and mergers between neutron stars and main sequence stars [5] have been proposed as sites for this nucleosynthesis process.

The $rp$ process starts at the breakout from the hot CNO cycle into the Ne-Na region, proceeding up the proton-rich side of stability via a series of proton-capture reactions and $\beta$ decays [2]. One of the nuclear reactions along the $rp$-process path, out of the Ne-Na region, is the $^{24}$Al$(p, \gamma)\,^{25}$Si reaction [6]. Variations in this rate affect relative end-point abundances of $^{28,29,30}$Si, $^{33,34}$S, and $^{36}$Ar in ONe novae [7]. In particular, the abundances of $^{29,30}$Si to $^{28}$Si are important in the identification of presolar grains in comets and asteroids [8].

The effect of nuclear isomers in astrophysical processes is not well understood. A recent theoretical study concluded that the presence of isomeric states in stellar nucleosynthesis scenarios can significantly impact the calculation of the reaction rates due to their unique nuclear properties [9]. Such is the case of the $^{24}$Al$(p, \gamma)\,^{25}$Si reaction. The existence of a low-lying isomeric state in $^{24}$Al ($^{24}$Al$^{m}$, $E_{ex} = 0.426$ MeV, $t_{1/2} = 130$ ms, $J^{\pi} = 1^{+}$) with a large difference in spin from the ground state ($^{24}$Al$^{gs}$, $t_{1/2} = 2.053$ h, $J^{\pi} = 4^{+}$) complicates the calculation of this reaction rate.

The main contribution to the $^{24}$Al$(p, \gamma)$ reaction rate proceeds through low-lying resonances above the proton separation energy in $^{25}$Si. It is expected that proton captures on $^{24}$Al$^{gs}$ and $^{24}$Al$^{m}$ proceed through different resonances in $^{25}$Si, therefore contributing separately to the rate of destruction of $^{24}$Al via proton-capture reactions, as was shown experimentally to be the case for the $^{26}$Al$^{m}(p, \gamma)\,^{27}$Si reaction [10,11].

In $rp$-process nucleosynthesis, $^{24}$Al is reached through the $^{23}$Mg$(p, \gamma)\,^{24}$Al reaction as well as the $^{22}$Mg$(p, \gamma)$ $^{23}$Al$(p, \gamma)\,^{24}$Si$(\beta)\,^{24}$Al reaction chain [2,5]. The correct calculation of the $^{24}$Al$^{m}(p, \gamma)\,^{25}$Si reaction rate is particularly important in the latter branch since the isomeric state in $^{24}$Al is strongly populated by the $\beta$ decay of $^{24}$Si, as shown by rate calculations of Refs. [9,12].

The $^{24}$Al$^{gs}(p, \gamma)\,^{25}$Si reaction rate has been the object of few previous studies. In the recent work by Longfellow *et al.* [6], states in $^{25}$Si were studied using $\gamma$-ray spectroscopy, refining the experimental information previously reported by Benenson *et al.* [13], and determining $\gamma$ decays and branching ratios for several excited states of $^{25}$Si. Above the proton separation threshold [$S_{p} = 3.414(10)$ MeV] in the region of astrophysical relevance, two states, a $9/2^{+}$ at $E_{ex} = 3.695(14)$ MeV and a $1/2^{+}$ at $E_{ex} = 3.802(11)$ MeV, were identified. The results of that study were used to constrain the rate of the $^{24}$Al$^{g}(p, \gamma)\,^{25}$Si reaction [6], showing that the contribution of the $9/2^{+}$ state was a factor of 10 higher than the one used in the previous network calculations performed by Herndl *et al.* [14]. Knapton [15] studied the $^{24}$Na$(d, p)\,^{25}$Na reaction to infer spectroscopic information on the mirror nucleus $^{25}$Si, with a beam that was 100% in the $^{24}$Na ground state. No information was previously available on the reactions of the $^{24}$Na isomeric state.

In this work, the $^{24}$Al$^{m}(p, \gamma)\,^{25}$Si reaction was studied via measurement of the $^{24}$Na$^{m}(d, p)\,^{25}$Na reaction using a $^{24}$Na beam with 90% of its content in its isomeric state. Spectroscopic information of states in $^{25}$Na populated by single-neutron transfer on the $^{24}$Na$^{m}$ was extracted. These states are mirror to states in $^{25}$Si populated by the $^{24}$Al$^{m}(p, \gamma)$ $^{25}$Si reaction. The reported experimental information constrains for the first time the destruction rate of $^{24}$Al via proton captures on its isomeric state.
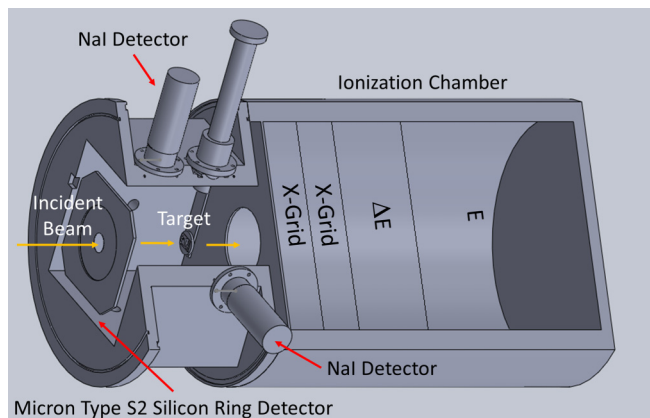
FIG. 1. Schematics of the experimental setup used during the present $^{24}$Na$(d, p)^{25}$Na experiment. The beam enters the reaction chamber from the left and is incident on a CD$_2$ target. Backward scattered protons from the interaction of the beam with the target are measured in a silicon S2 detector. The heavy products as well as the unreacted beam are measured downstream in an ionization chamber. Two NaI detectors were placed outside the reaction chamber at $\sim 90°$ from the target position and are used to monitor the isomeric content of the beam via detection of the 472-keV $\gamma$ rays.

## II. EXPERIMENT

The measurement of the $^{24}$Na$^m(d, p)^{25}$Na reaction was performed at the John D. Fox Accelerator Laboratory at Florida State University. A primary beam of stable $^{23}$Na was accelerated by the FN Tandem Van de Graff accelerator followed by the linear accelerator (LINAC) to an energy of 115 MeV. The primary $^{23}$Na beam was then sent to the RESO-LUT radioactive beam facility [16], where it was incident on a production target filled with deuterium gas to produce a radioactive beam of $^{24}$Na via the $^{23}$Na$(d, p)^{24}$Na reaction in-flight [17]. The production target was 40 mm long, with a 2.5-micron HAVAR entrance and exit windows, was cooled with liquid nitrogen to 77 K, and was kept at 350 Torr.

The resultant $^{24}$Na beam was then tuned using the focusing elements of RESOLUT and sent downstream to the reaction chamber. The $11^+$ charge state of $^{24}$Na arrived at the target position with 85.5 MeV. The main contaminant of the beam was the $10^+$ charge state of the primary $^{23}$Na at 73.8 MeV.

The beam was incident on a 517-$\mu$g/cm$^2$ CD$_2$ target. In the reaction chamber, a double-sided 300-$\mu$m-thick Micron S2 silicon detector was placed 10.5 cm upstream from the target position to measure charged reaction particles at backward angles. The angular coverage of the silicon detector was $161.6°$–$173.7°$ in the laboratory frame. Outside of the reaction chamber, two sodium iodide (NaI) detectors were placed close to $90°$ above and to the side of the target position to monitor the isomeric content of the beam via the detection of the 472-keV $\gamma$ rays from the decay of the isomeric state to the ground state ($t_{1/2} = 20.18$ ms) of the $^{24}$Na beam [18]. Downstream from the target position, an ionization chamber collected the unreacted beam as well as the heavy reactants. The ionization chamber had an 8-micron Kapton window and consisted of two 40-mm position-sensitive sections, an 80-mm
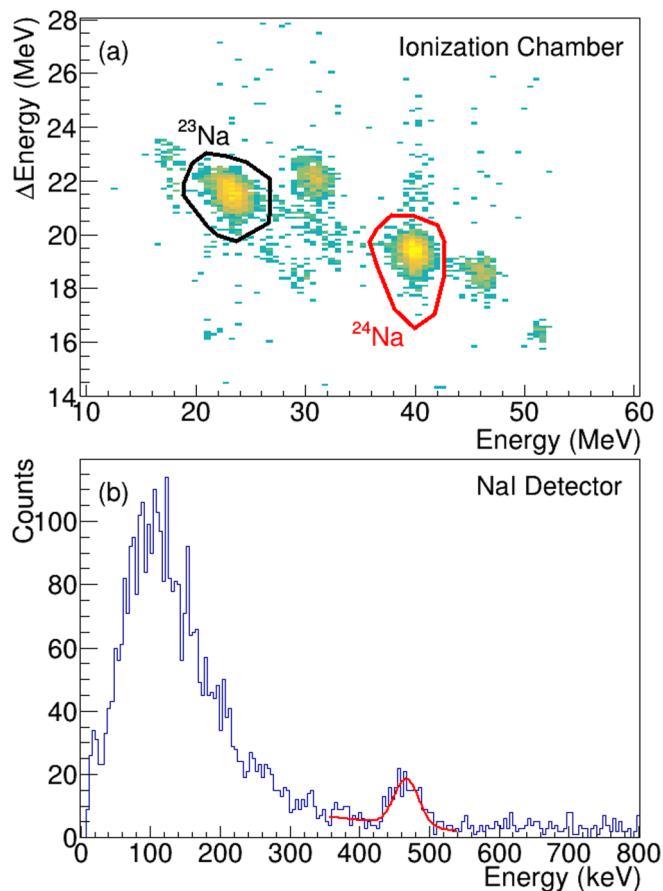


FIG. 2. (a) Ionization chamber spectrum for a no-target 2-min run. The $^{24}$Na beam as well as its main contaminant, the primary $^{23}$Na beam, are indicated. The ratio of $^{23}$Na to $^{24}$Na was about 1:1. (b) Typical spectrum of one of the NaI detectors taken during a gold-target 2-min run. The peak indicated in red correspond to the 472-keV $\gamma$ ray in $^{24}$Na which was used to determine and monitor the isomeric content of the beam.

section to measure energy loss ($\Delta E$), and a 200-mm section to fully stop the beam (E). The ionization chamber was filled with isobutane and was kept at a pressure of 45 Torr. The two position-sensitive sections were not used in the analysis of this experiment. A schematics of the experimental setup is shown in Fig. 1.

The $^{24}$Na beam and its main contaminant, the primary $^{23}$Na beam, were well separated in the ionization chamber by their energy losses, as shown in Fig. 2(a). Time-of-flight information from the production target to the detectors was also used to differentiate the beam components. The ratio of $^{24}$Na to $^{23}$Na measured in the ionization chamber throughout the experiment was approximately 1:1.

The isomeric content of the beam was determined using sets of 2-min synchronized runs taken at various points during the experiment. For this purpose, a thick gold target was placed at the target position to fully stop the beam. The NaI detectors, placed close to $90°$ directly outside the reaction chamber, measured the 472-keV $\gamma$ rays characteristic of the decay of the isomeric state in $^{24}$Na to its ground
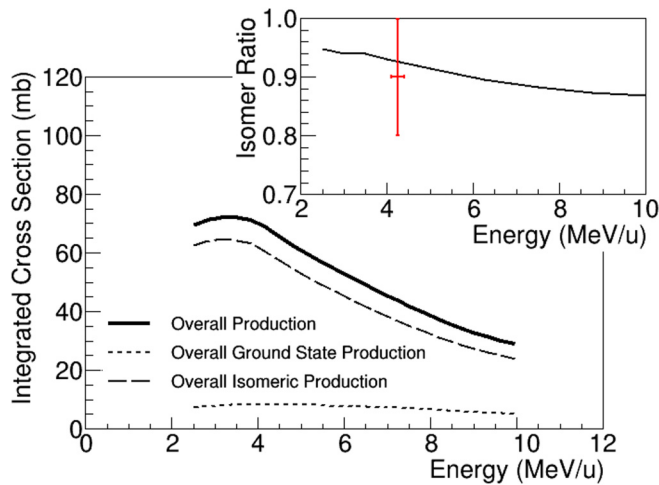
FIG. 3. DWBA calculations for the production of a $^{24}$Na beam via the $^{23}$Na$(d, p)^{24}$Na reaction. The production cross section as a function of the beam energy for the ground state (short dashed line), isomeric state (long dashed line), and total production of $^{24}$Na (solid line) are shown. In the inset, the DWBA calculated isomer ratio, or isomer to total ratio, is shown by the solid black line. The experimentally determined isomeric ratio is shown by the single point. Good agreement is observed between DWBA calculations and the experimental data point.

state. Figure 2(b) shows a typical spectrum obtained with one of the NaI detectors during a gold-target run. A peak corresponding to the 472-keV $\gamma$ ray is observed. A no-target run immediately followed the gold-target measurement. The target was removed allowing the full beam to pass directly to the ionization chamber to measure the total amounts of $^{23}$Na and $^{24}$Na. Figure 2(a) shows a typical spectrum taken in the ionization chamber with no target. Additionally, during the no-target runs the NaI detectors measured the background $\gamma$ rays in order to filter out any non-target-related contributions to the 472-keV $\gamma$-ray spectrum. After the experiment, calibrated sources were placed at the target position to obtain the absolute efficiencies of the NaI detectors. From the sets of synchronized runs, it was determined that 90% $\pm$ 10% of the $^{24}$Na beam was in the isomeric state.

In order to confirm the experimentally obtained isomeric content of the beam, distorted wave Born approximation (DWBA) calculations were also performed for the $^{23}$Na$(d, p)^{24}$Na reaction. The DWBA code Fresco [19] was utilized to perform these calculations. The optical model parameters for the incoming $^{23}$Na $+$d and outgoing $^{24}$Na $+$p channels were taken from Ref. [20].

The overall DWBA calculated yields for the isomeric and ground states in $^{24}$Na as well as the DWBA calculated isomeric content are shown in Fig. 3. The experimentally determined isomeric content is also shown. There is good agreement between the experimental measurement and the DWBA calculated yields of the isomeric ratio. In addition, the DWBA calculations show that as the energy varies, the isomeric content of the beam varies smoothly; thus small changes in the production energy will have no significant effect in the overall isomeric content of the beam. This observation
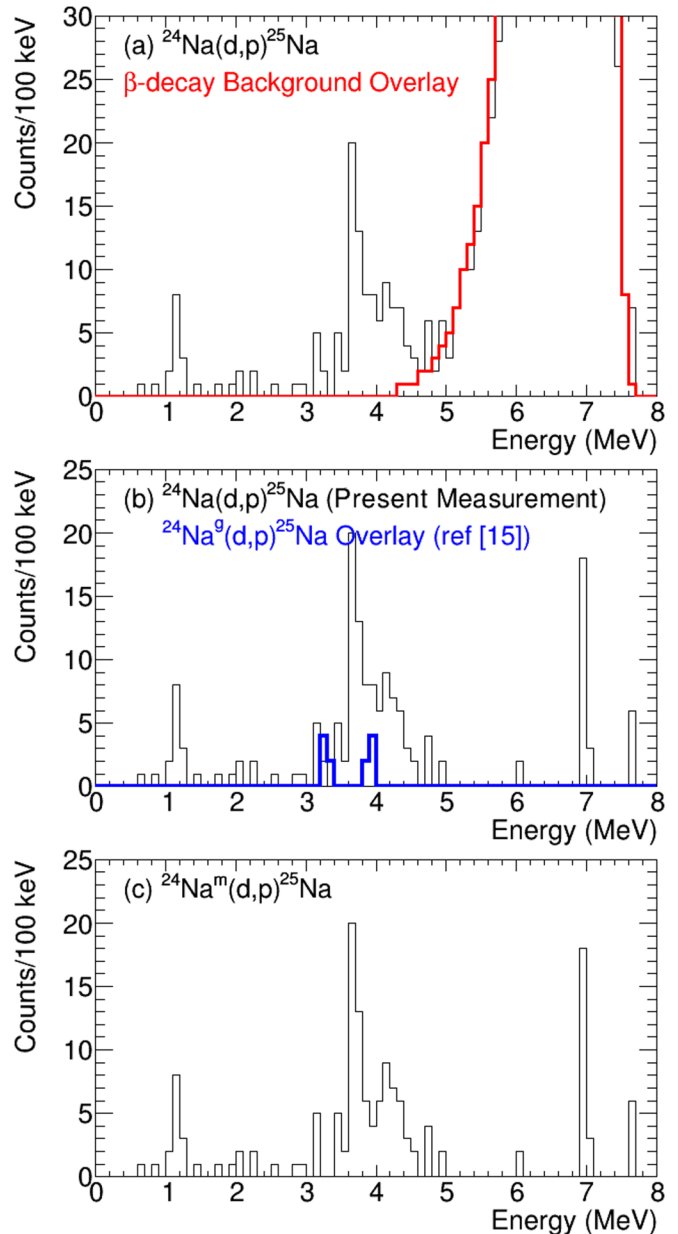


FIG. 4. $^{25}$Na apparent excitation energy spectrum from the $^{24}$Na$(d, p)^{25}$Na reaction using the $Q$ value from the isomeric state, in the angular range of $\theta_{lab} = 161.6°$–$173.7°$, measured in the present work. (a) The spectrum for states in $^{25}$Na populated in the present $^{24}$Na$(d,p)$ reaction. The contribution of $\beta$-decay background from the decay of the $^{24}$Na$^{gs}$ to $^{24}$Mg, scaled to fit the data (red thick line), is observed at energies above 5 MeV. (b) $^{25}$Na apparent excitation energy spectrum after the subtraction of the $\beta$-decay background contribution. The contribution from the ground state component of the beam is also shown (blue thick line). The ground state contribution was estimated from the work of Ref. [15]. Given the kinematics used ($Q$ value of the isomeric state), states populated by the ground state appear shifted up in energy by 472 keV. (c) The $^{25}$Na excitation energy spectrum populated by the $^{24}$Na$^m(d, p)^{25}$Na reaction populated with only the isomeric component of the beam.

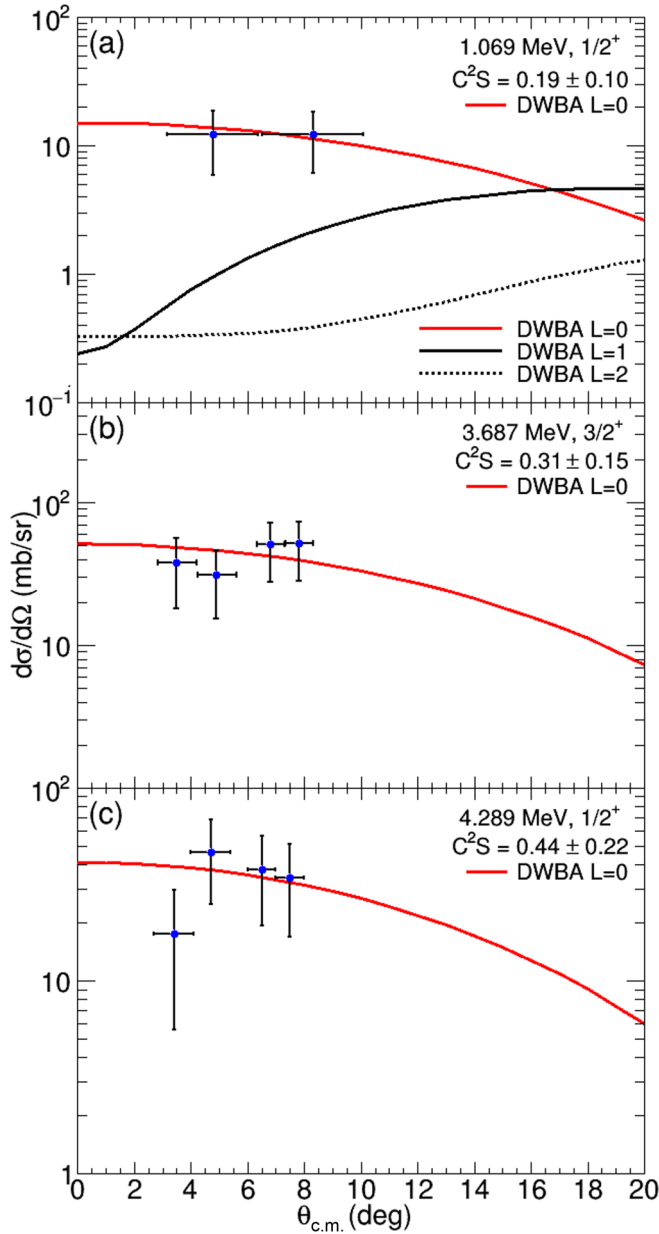contrasts that of the production of an isomeric beam in $^{26}$Al ($^{26}$Al$^m$) via the $^{26}$Mg$(p,n)$ reaction [21].

FIG. 5. Angular distributions for the states populated in the present $^{24}\text{Na}^m(d, p)^{25}\text{Na}$ reaction at (a) $E_{ex} = 1.069$ MeV ($1/2^+$), (b) $E_{ex} = 3.687$ MeV ($3/2^+$), and (c) $E_{ex} = 4.289$ MeV ($1/2^+$). All three states show $\ell = 0$ neutron transfers from the $1^+$ isomeric state in $^{24}\text{Na}$. DWBA calculations were used to fit the experimental data. A chi-square minimization was used to determine the best value for the spectroscopic factors ($C^2S$).

The $^{24}\text{Na}(d, p)^{25}\text{Na}$ reaction was measured using a 517-$\mu\text{g/cm}^2$-thick $CD_2$ target which was bombarded with a 85.5-MeV $^{24}\text{Na}$ beam. The absolute normalization of the $^{24}\text{Na}$ beam was performed using the $^{23}\text{Na}(d, p)^{24}\text{Na}$ reaction, which has been previously studied in Refs. [20,22] and which was measured through the $^{23}\text{Na}$ component of the beam. Two states strongly populated by the $^{23}\text{Na}(d,p)$ reaction in $^{24}\text{Na}$ at $E_{ex} = 1.34$ MeV, $J^\pi = 1^+$ and $E_{ex} = 1.846$ MeV, $J^\pi = 2^+$ were observed in the silicon detector when gating on the $^{23}\text{Na}$ beam component.

TABLE I. Spectroscopic factors for states observed in the $^{24}\text{Na}^m(d, p)^{25}\text{Na}$ reaction. Both experimentally determined and USDB shell model spectroscopic factors are shown. For shell model states, only spectroscopic factors greater than 0.075 are considered.

| Excitation energy (MeV) | $J^\pi$ | Experiment $C^2S$ $\ell = 0$ | USDB SM $C^2S$ $\ell = 0$ | $\ell = 2$ |
|---|---|---|---|---|
| 1.069 | $1/2^+$ | $0.19 \pm 0.10$ | 0.303 | 0.001 |
| 3.687 | $3/2^+$ | $0.31 \pm 0.15$ | 0.253 | 0.145 |
| 3.955 | $(3/2^+)$[a] | | 0.095 | 0.016 |
| 4.289 | $1/2^+$ | $0.44 \pm 0.22$ | 0.329 | 0.017 |

[a]Spin from shell model calculations.

Cross sections for these states were extracted and normalized using DWBA calculations, with the optical model parameters and spectroscopic factors given in Refs. [20,22]. The total amount of the $^{23}\text{Na}$ beam was then obtained by taking into account the target thickness and solid angle coverage of the silicon detector in the present experiment for both states. The absolute $^{24}\text{Na}$ beam normalization was then calculated using the $^{24}\text{Na}$-to-$^{23}\text{Na}$ ratio measured throughout the experiment in the ionization chamber. The typical intensity of the $^{24}\text{Na}$ beam was determined to be $\sim$800 pps.

## III. RESULTS

States in $^{25}\text{Na}$ populated in the present experiment via the $^{24}\text{Na}(d,p)$ reaction with a beam of $^{24}\text{Na}$ with 90% of its content in its isomeric $1^+$ state were measured in the silicon detector in the angular range of $\theta_{\text{lab}} = 161.6°–173.7°$. The energy of the measured protons was then converted to apparent excitation energy in $^{25}\text{Na}$ using the $Q$ value of the isomeric state in $^{24}\text{Na}$.

Figure 4(a) shows the $^{25}\text{Na}$ apparent excitation energy spectrum obtained in the present experiment. A large background peak can be seen at energies above 5 MeV (low measured energies). This background peak arises from the $\beta$ decay of the $^{24}\text{Na}^{gs}$ to $^{24}\text{Mg}$. Although most of the beam is in the $^{24}\text{Na}$ isomeric state, it decays to the ground state in $^{24}\text{Na}$ via the emission of a 472-keV $\gamma$ ray with $t_{1/2} = 20.18$ ms, where it subsequently $\beta$-decays to $^{24}\text{Mg}$ with $t_{1/2} = 14.997$ h. Over the course of the experiment, $^{24}\text{Na}$ in the ground state accumulated in the reaction chamber, providing the source of this $\beta$-decay background.

A run with no beam on target was taken to measure the $\beta$-decay background in the silicon detector. The shape of the $\beta$-decay spectrum shows good agreement with the high-energy structure in the excitation energy spectrum. This background spectrum was then scaled to the peak observed in the high-energy portion of the excitation energy spectrum (red solid line) and subtracted. Figure 4(b) shows the apparent excitation energy spectrum with the $\beta$-decay background subtracted.

The contribution of the ground state component of the $^{24}\text{Na}$ beam (10% of the total $^{24}\text{Na}$ beam content) was estimated using the results from Ref. [15], where the $^{24}\text{Na}(d,p)$ reaction was measured using a pure $^{24}\text{Na}^{gs}$ beam. From that work's results, we estimated that contributions from the ground state
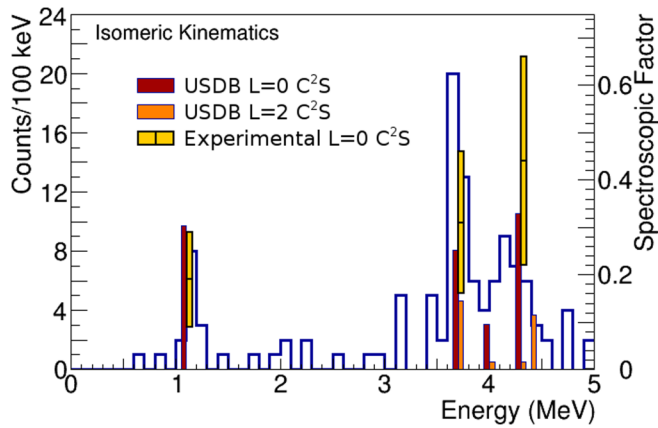
FIG. 6. $^{25}$Na apparent excitation energy. The states in $^{25}$Na populated in the present $^{24}$Na$^m(d, p)$ $^{25}$Na reaction in the energy range $E_{cm} = 0$–5 MeV are compared with shell model predictions using the USDB interaction. Spectroscopic factors (right $y$ axis) extracted from fits to the experimental data (yellow bars) and predicted by the shell model (dark red bars for $\ell = 0$ transfers, orange for $\ell = 2$) are overlaid.

component of the beam were negligible given the low intensity of our $^{24}$Na beam. The estimated contribution of the $^{24}$Na$^{gs}(d, p)$ $^{25}$Na to the present experiment is also shown in Fig. 4(b) (blue solid line). The $^{25}$Na apparent excitation energy spectrum from our present $^{24}$Na$^m(d, p)$ $^{25}$Na measurement is shown in Fig. 4(c), where both contributions from the

$\beta$-decay background and the ground state component of the beam have been subtracted.

The results in Fig. 4 show the high selectivity in the states populated in the present $^{24}$Na$^m(d, p)$ $^{25}$Na measurement. Three states are observed to be populated by the isomeric $^{24}$Na beam, plus a fourth possible state. The three observed states are identified as the 1.069-MeV $J^\pi = 1/2^+$ state, the 3.687-MeV $J^\pi = 3/2^+$ state, and the 4.289-MeV $J^\pi = 1/2^+$ state. Angular distributions for these strongly populated states were fitted using DWBA calculations with the code FRESCO [19]. For the incoming and outgoing channels, optical model potential parameters were taken from Refs. [23,24]. Figure 5 shows the angular distributions for these three states along with the DWBA fits to the angular distributions. The spectroscopic factors were extracted using a chi-square fit to the experimental data and are listed in Table I. Even with the limited statistics of the present experiment, the angular distributions confirm that $\ell = 0$ transfers are selectively populated in the present reaction.

Shell model calculations were also performed using the USDB interaction [25,26]. From these calculations, good agreement is found between the energies and spectroscopic factors of states predicted by the shell model and the three observed states in the present experiment. Good agreement is also obtained between the experimentally extracted spectroscopic factors and those predicted by the shell model. A comparison between states and energies extracted from the experiment and with shell model calculations is shown in Fig. 6 and listed in Table I. The additional fourth possible
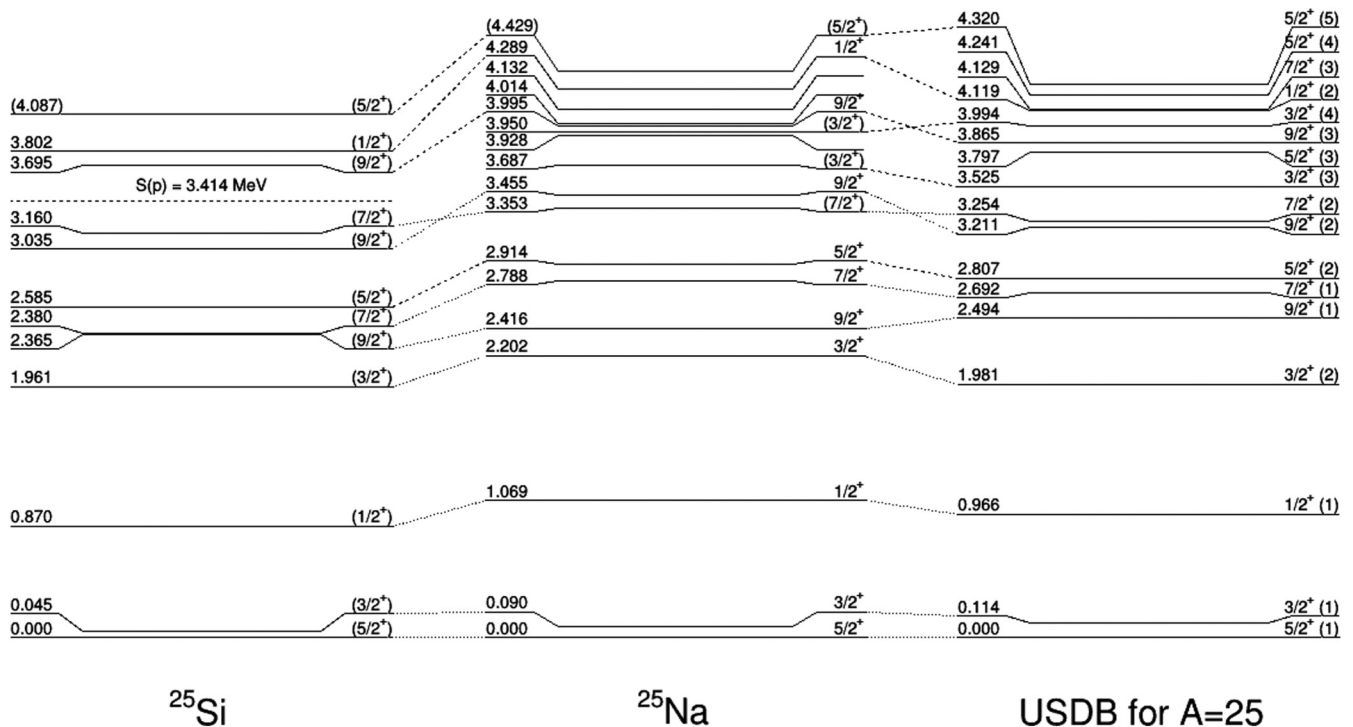


FIG. 7. Level schemes for $^{25}$Si and $^{25}$Na, and USDB shell model calculations for the A = 25 system. Level information for $^{25}$Si and $^{25}$Na taken from Refs. [6,18,27]. USDB level information from [25]. The dotted lines indicate mirror levels determined by Ref. [13]. The dashed lines indicate proposed mirror levels. The energies of the $5/2^+$ state at 4.087 MeV in $^{25}$Si and 4.429 MeV in $^{25}$Na are based on the USDB shell model calculations with Thomas-Ehrman shifts of $-0.479$ MeV and 0.224 MeV, respectively [28,29].

state at $E_{ex} = 3.950$ MeV has previously been reported in Refs. [18,27]. Using shell model calculations, this state is expected to be a $3/2^+$ state. Figure 6 shows the apparent excitation energy spectrum for states populated by the isomeric component of the beam with bars for the spectroscopic factors overlayed. The yellow bars show the spectroscopic factors for the experimentally observed $\ell = 0$ transfers, and the dark red and orange bars show the shell model calculated spectroscopic factors for $\ell = 0$ and $\ell = 2$ transfers, respectively.

The high selectivity of the present data allows us to propose mirror level assignments for states in the $^{25}$Na - $^{25}$Si system. A diagram of the states in $^{25}$Na, $^{25}$Si, and shell model calculations with mirror level assignments using data from Refs. [6,13,18,25,27] is shown in Fig. 7. For the shell model states, only those with $C^2S > 0.075$ were used. The observed $1/2^+$ states in $^{25}$Na at $E_{ex} = 1.069$ MeV and $E_{ex} = 4.289$ MeV are the mirror levels of states in $^{25}$Si at $E_{ex} = 0.87$, and $E_{ex} = 3.802$ MeV with spectroscopic factors for an $\ell = 0$ transfer of $C^2S = 0.19$ and $0.44$, respectively. The mirror level of the $E_{ex} = 3.687$ MeV state in $^{25}$Na ($\ell = 0$ $C^2S = 0.31$) has not been observed in $^{25}$Si. These states are predicted by shell model calculations [25].

## IV. ASTROPHYSICAL IMPLICATIONS

In order to evaluate the contribution of the $1^+$ isomeric state in $^{24}$Al to the $^{24}$Al$(p, \gamma)^{25}$Si reaction rate, we focused on the states in $^{25}$Na that are mirrors to the states above the proton threshold in $^{25}$Si ($S_p = 3.414$ MeV) which are expected to dominate the astrophysical rate of the $^{24}$Al$(p, \gamma)^{25}$Si reaction.

The observed $1/2^+$ state at $E_{ex} = 4.289$ MeV in $^{25}$Na is a mirror to the one at $E_{ex} = 3.802$ MeV in $^{25}$Si. After taking into account the energy of the isomeric state of $^{24}$Al ($E_{ex} = 0.426$ MeV), we find an energy with respect to the isomer of $E_r^m = -0.038$ MeV, making it a subthreshold resonance. The contribution of this state to the reaction rate was calculated using a Breit-Wigner subthreshold resonance formalism as described by Refs. [30,31]. The effect of this $1/2^+$ subthreshold resonance is shown by the red line in Fig. 8(a), where the ratio of the rate calculated of the $1/2^+$ resonance state at $E_r^m = -0.038$ MeV in $^{25}$Si to that of the current ground state REACLIB rate is shown for a temperature range from 0.01 to 10 GK.

In addition to our experimentally observed states, the USDB shell model calculation [25,26] predicts a $5/2^+$ state that could contribute to the $^{24}$Al$^m(p, \gamma)^{25}$Si reaction rate. Using a Thomas-Ehrman shift of 0.479 MeV on the proton single-particle energy, we placed the unobserved state at $E_{ex} = 4.087$ MeV in $^{25}$Si [28,29]. Accounting for the energy of the isomeric state of $^{24}$Al ($E_{ex} = 0.426$ MeV), we find a resonance energy with respect to the isomer of $E_r^m = 0.247$ MeV. The mirror $5/2^+$ state would be at $E_{ex} = 4.429$ MeV in $^{25}$Na. Due to the low statistics of the present experiment, and that this state would be populated by an $\ell = 2$ transfer from the $1^+$ isomer, we are unable to identify this state which would be at the background level in our data. The shell model spectroscopic factor for $\ell = 2$ transfer to this state was found to be $C^2S = 0.115$ [25]. The resonance strength of such resonance was calculated according to Ref. [32] and was found to
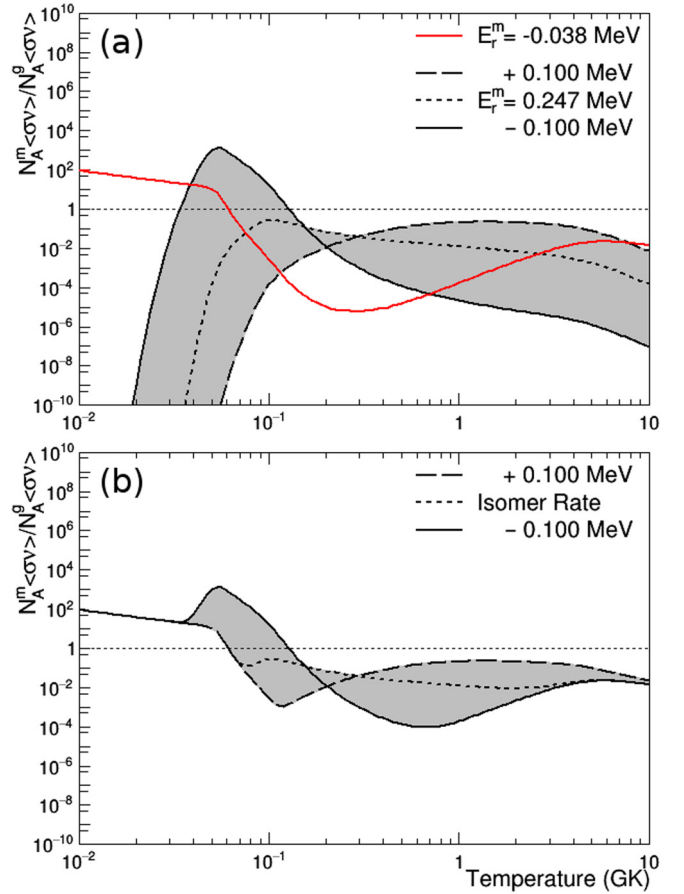


FIG. 8. Ratio of the isomeric rates extracted in this work to the current ground state REACLIB rate [34]. (a) Individual isomeric rate contributions. The $1/2^+$ subthreshold resonance at $E_r^m = -0.038$ MeV (red line) and the $5/2^+$ state at $E_r^m = 0.247$ MeV (black lines) as a function of the temperature. The resonance energy of the $5/2^+$ resonance was varied by $\pm 100$ keV (shaded area). (b) Total isomeric contribution ($1/2^+ + 5/2^+$) determined in this work. The shaded area indicates the uncertainty in the energy of the $5/2^+$ resonance.

be $\omega\gamma = 0.735$ meV. The effect this resonance as well as the uncertainty in the resonance energy are indicated by the black lines in Fig. 8(a), where the ratio of the rate calculated with the shell model predicted a $5/2^+$ resonance state at $E_r^m = 0.247$ MeV in $^{25}$Si to that of the current ground state REACLIB rate as a function of temperature is plotted. The energy of the predicted resonance has been varied by $\pm 100$ keV to determine possible effects of a shift in its location and it is shown by the shaded region (the change in resonance energy also changes the calculated resonance strength). This variation in the energy was chosen based on the resonance energy uncertainty given in the network calculations of Ref. [33] for the same state when populated by the ground state.

The ratio of the total isomeric contributions of the $^{24}$Al$(p, \gamma)^{25}$Si reaction rate determined in this work to the ground state contributions is shown in Fig. 8(b). The upper and lower limits here are due to the uncertainty in the energy of the $5/2^+$ shell model predicted resonance.
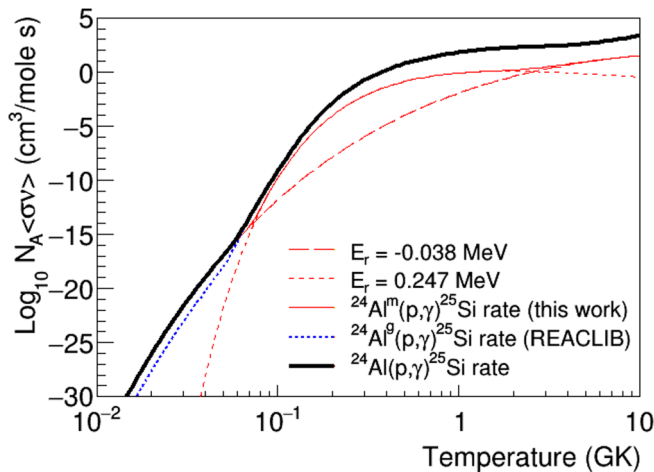
FIG. 9. The rate of the $^{24}$Al$(p, \gamma)\,^{25}$Si reaction. The red lines show the contributions from the $1^+$ isomeric state in $^{24}$Al presented in this work, while the blue line shows the current recommended REACLIB rate [34] with the state from the work of Ref. [6] added in. The black line denotes the total rate of the $^{24}$Al$(p, \gamma)\,^{25}$Si.

The present calculated rate for the $^{24}$Al$^m(p, \gamma)\,^{25}$Si reaction is shown in Fig. 9. The red lines show the rate for both the experimentally measured subthreshold $1/2^+$ state at $E_r^m = -0.038$ MeV in $^{25}$Si (red long dashed line), and the shell model predicted $5/2^+$ state at $E_r^m = 0.247$ MeV in $^{25}$Si (red short dashed line), as well as their total combined contribution to the $^{24}$Al$^m(p, \gamma)\,^{25}$Si reaction rate (red solid line). The current REACLIB ground state rate [14,35] with the recent work of Ref. [6] is also included for comparison (blue dotted line).

In the temperature range of interest to the $rp$ process $0.1 \leqslant T_9 \leqslant 10$ [1,2,5], the contribution of the subthreshold state in $^{25}$Si to the rate of the $^{24}$Al$(p, \gamma)\,^{25}$Si rate is negligible. For the shell model predicted resonance state placed at $E_r^m = 0.247$ MeV in $^{25}$Si, it is observed that its influence to the total reaction rate depends on the exact location of its resonance

energy, as shown in Fig. 8(b). Since variations in the energy of this state will cause the overall contribution to change, further measurements are needed to confirm the existence and location of this state as well as the strength of the resonance to fully determine its influence to the rate of the $^{24}$Al$(p, \gamma)\,^{25}$Si reaction when populated by the isomeric state.

## V. SUMMARY

In summary, a radioactive beam of $^{24}$Na with 90% of its content in the isomeric $1^+$ state was developed, characterized, and used to perform, for the first time, a measurement of the $^{24}$Na$^m(d, p)\,^{25}$Na reaction at Florida State University's John D. Fox Accelerator Laboratory. States in $^{25}$Na up to $E_{ex} = 5$ MeV in excitation energy, populated by $\ell = 0$ transfers from the isomeric state in $^{24}$Na, were selectively observed in this experiment. Spectroscopic information extracted from this experiment was compared with USDB shell model calculations and showed good agreement between experiment and theory.

Mirror symmetry arguments between $^{25}$Na and $^{25}$Si were used to provide spectroscopic information of states above the proton threshold in $^{25}$Si and, for the first time, constrain the contribution of the isomeric $1^+$ state in $^{24}$Al to the rate of the $^{24}$Al$(p, \gamma)\,^{25}$Si reaction. The contribution of an $\ell = 0$ subthreshold resonance was determined to be negligible. The presence of an additional $\ell = 2$ resonance, predicted by the shell model but not observed in the present experiment, could have a role in the $^{24}$Al$(p, \gamma)\,^{25}$Si reaction rate. Experimental information on the exact location of this state in $^{25}$Si is needed to evaluate its impact to the $^{24}$Al$(p, \gamma)\,^{25}$Si reaction rate.

[1] R. Wallace and S. E. Woosley, Explosive hydrogen burning, Astrophys. J., Suppl. Ser. **45**, 389 (1981).

[2] J. L. Fisker, H. Schatz, and F.-K. Thielemann, Explosive hydrogen burning during type I x-ray bursts, Astrophys. J., Suppl. Ser. **174**, 261 (2008).

[3] H. Schatz and K. Rehm, X-ray binaries, Nucl. Phys. A **777**, 601 (2006).

[4] Z. Meisel, A. Deibel, L. Keek, P. Shternin, and J. Elfritz, Nuclear physics of the outer layers of accreting neutron stars, J. Phys. G: Nucl. Part. Phys. **45**, 093001 (2018).

[5] L. Van Wormer, J. Görres, C. Iliadis, M. Wiescher, and F.-K. Thielemann, Reaction rates and reaction sequences in the rp-process, Astrophys. J. **432**, 326 (1994).

[6] B. Longfellow, A. Gade, B. A. Brown, W. A. Richter, D. Bazin, P. C. Bender, M. Bowry, B. Elman, E. Lunderberg, D. Weisshaar, and S. J. Williams, Measurement of key resonances

for the $^{24}$Al$(p, \gamma)^{25}$Si reaction rate using in-beam $\gamma$-ray spectroscopy, Phys. Rev. C **97**, 054307 (2018).

[7] C. Iliadis, A. Champagne, J. Jose, S. Starrfield, and P. Tupper, The effects of thermonuclear reaction-rate variations on nova nucleosynthesis: A sensitivity study, Astrophys. J., Suppl. Ser. **142**, 105 (2002).

[8] D. D. Clayton and L. R. Nittler, Astrophysics with presolar stardust, Annu. Rev. Astron. Astrophys. **42**, 39 (2004).

[9] G. W. Misch, S. K. Ghorui, P. Banerjee, Y. Sun, and M. R. Mumpower, Astromers: Nuclear isomers in astrophysics, Astrophys. J., Suppl. Ser. **252**, 2 (2020).

[10] C. M. Deibel, J. A. Clark, R. Lewis, A. Parikh, P. D. Parker, and C. Wrede, Toward an experimentally determined $^{26}$Al$^m(p, \gamma)^{27}$Si reaction rate in one novae, Phys. Rev. C **80**, 035806 (2009).

[11] S. Almaraz-Calderon, K. E. Rehm, N. Gerken, M. L. Avila, B. P. Kay, R. Talwar, A. D. Ayangeakaa, S. Bottoni, A. A. Chen, C. M. Deibel, C. Dickerson, K. Hanselman, C. R. Hoffman, C. L. Jiang, S. A. Kuvin, O. Nusair, R. C. Pardo, D. Santiago-Gonzalez, J. Sethi, and C. Ugalde, Study of the $^{26}Al^{m}(d, p)^{27}Al$ Reaction and the Influence of the $^{26}Al\,0^{+}$ Isomer on the Destruction of $^{26}Al$ in the Galaxy, Phys. Rev. Lett. **119**, 072701 (2017).

[12] G. W. Misch (private communication).

[13] W. Benenson, J. Driesbach, I. D. Proctor, G. F. Trentelman, and B. M. Preedom, Energy levels of $^{25}Si$ from the reaction $^{28}Si(^{3}He, ^{6}He)^{25}Si$ at 70.4 MeV, Phys. Rev. C **5**, 1426 (1972).

[14] H. Herndl, J. Görres, M. Wiescher, B. A. Brown, and L. Van Wormer, Proton capture reaction rates in the rp process, Phys. Rev. C **52**, 1078 (1995).

[15] A. J. Knapton, Structure of $^{25}Na$ measured using $d(^{24}Na, p)^{25}Na$ with a radioactive $^{24}Na$ beam, Ph.D. thesis, University of Surrey, 2017.

[16] I. Wiedenhöver, L. Baby, D. Santiago-Gonzalez, A. Rojas, J. Blackmon, G. Rogachev, J. Belarge, E. Koshchiy, A. Kuchera, L. Linhardt *et al.*, Studies of exotic nuclei at the RESOLUT facility of Florida State University, in *Fission and Properties of Neutron-Rich Nuclei* (World Scientific, Singapore, 2014), pp. 144–151.

[17] B. Harss, R. C. Pardo, K. E. Rehm, F. Borasi, J. P. Greene, R. V. F. Janssens, C. L. Jiang, J. Nolen, M. Paul, J. P. Schiffer, R. E. Segel, J. Specht, T. F. Wang, P. Wilt, and B. Zabransky, Production of radioactive ion beams using the in-flight technique, Rev. Sci. Instrum. **71**, 380 (2000).

[18] National nuclear data center, https://www.nndc.bnl.gov/

[19] Fresco coupled reaction channels calculations, http://www.fresco.org.uk/

[20] C. Daum, The $^{23}Na(d, p)^{24}Na$ reaction and the nuclear structure of $^{24}Na$, Nucl. Phys. **45**, 273 (1963).

[21] B. Asher, S. Almaraz-Calderon, O. Nusair, K. Rehm, M. Avila, A. Chen, C. Dickerson, C. Jiang, B. Kay, R. Pardo, D. Santiago-Gonzalez, and R. Talwar, Development of an isomeric beam of $^{26}Al$ for nuclear reaction studies, Nucl. Instrum. Methods Phys. Res., Sect. A **899**, 6 (2018).

[22] C. Daum, The nuclear structure of $^{24}Na$ and some remarks on the nuclear structure of $^{25}Mg$, Nucl. Phys. **51**, 244 (1964).

[23] Y. Han, Y. Shi, and Q. Shen, Deuteron global optical model potential for energies up to 200 MeV, Phys. Rev. C **74**, 044615 (2006).

[24] A. Koning and J. Delaroche, Local and global nucleon optical models from 1 kev to 200 MeV, Nucl. Phys. A **713**, 231 (2003).

[25] A. Volya (private communication).

[26] W. A. Richter, S. Mkhize, and B. A. Brown, *sd*-shell observables for the USDA and USDB Hamiltonians, Phys. Rev. C **78**, 064302 (2008).

[27] J. M. VonMoss, S. L. Tabor, V. Tripathi, A. Volya, B. Abromeit, P. C. Bender, D. D. Caussyn, R. Dungan, K. Kravvaris, M. P. Kuchera, R. Lubna, S. Miller, J. J. Parker, and P.-L. Tai, Higher-spin structures in $^{21}F$ and $^{25}Na$, Phys. Rev. C **92**, 034301 (2015).

[28] R. G. Thomas, On the determination of reduced widths from the one-level dispersion formula, Phys. Rev. **81**, 148 (1951).

[29] J. B. Ehrman, On the displacement of corresponding energy levels of C13 and N13, Phys. Rev. **81**, 412 (1951).

[30] C. E. Rolfs and W. S. Rodney, *Cauldrons in the Cosmos: Nuclear Astrophysics* (University of Chicago Press, Chicago, IL, 1988).

[31] C. Angulo, M. Arnould, M. Rayet, P. Descouvemont, D. Baye, C. Leclercq-Willain, A. Coc, S. Barhoumi, P. Aguer, C. Rolfs, R. Kunz, J. Hammer, A. Mayer, T. Paradellis, S. Kossionides, C. Chronidou, K. Spyrou, S. Degl'Innocenti, G. Fiorentini, B. Ricci *et al.*, A compilation of charged-particle induced thermonuclear reaction rates, Nucl. Phys. A **656**, 3 (1999).

[32] R. Longland, C. Iliadis, A. Champagne, J. Newton, C. Ugalde, A. Coc, and R. Fitzgerald, Charged-particle thermonuclear reaction rates: I. Monte Carlo method and statistical distributions, Nucl. Phys. A **841**, 1 (2010).

[33] C. Iliadis, R. Longland, A. Champagne, and A. Coc, Charged-particle thermonuclear reaction rates: III. Nuclear physics input, Nucl. Phys. A **841**, 251 (2010).

[34] R. H. Cyburt, A. M. Amthor, R. Ferguson, Z. Meisel, K. Smith, S. Warren, A. Heger, R. D. Hoffman, T. Rauscher, A. Sakharuk, H. Schatz, F. K. Thielemann, and M. Wiescher, The JINA REACLIB database: Its recent updates and impact on type-I x-ray bursts, Astrophys. J., Suppl. Ser. **189**, 240 (2010).

[35] C. Iliadis, R. Longland, A. Champagne, A. Coc, and R. Fitzgerald, Charged-particle thermonuclear reaction rates: II. Tables and graphs of reaction rates and probability density functions, Nucl. Phys. A **841**, 31 (2010).